出國報告(出國類別:出席國際研討會)

The 8th International Conference On Technological Advances Of Thin Films and Surface Coatings (Thin Films 2016)

國際學術研討會

出國公差報告

服務機關：國立虎尾科技大學

姓名職稱：楊東昇 教授

派赴國家：新加坡

出國期間：2016.07.11-2016.07.16

報告日期：2016.10.20

摘要

本次出國參與研討會之目的在於提升研究成果之國際交流與精進研究方法。經由參加『The 8th International Conference On Technological Advances Of Thin Films and Surface Coatings (Thin Films 2016)』國際學術研討會議，且與參與之其他國家之學者進行交流，並了解目前薄膜與鍍層先進技術及其應用，得到國際交流的能量。

目次

一、 目的

本次參與新加坡所舉辦之國際研討會之目的為與國際有關薄膜與鍍層先進技術及其應用之國際學者交流且發表論文，並藉由互相交流之過程拓展國際合作之契機。

二、 過程

此次國際研討會為 105 年 07 月 12 日至 105 年 07 月 15 日於新加坡舉行，因此本人於 103 年 07 月 11 日啟程、07 月 12-15 日參加研討會及 07 月 16 日返程共六日請公差假，簽呈圖一。圖二為此研討會會場上之大型海報，圖三為此研討會海報上之議程，圖四為本人參加研討會之論文海報及參與研討會相片，會議中除了進行發表論文且與學者進行交流。圖五為研討會論文集之摘要，圖六為此次發表文章之內容，硬質鍍膜技術已廣泛應用於切削、成形模具等機械製造業，藉此來改 善其磨耗特性、提高模具的壽命及降低生產成本，市面上以氮化鈦(TiN)、 氮化鉻(CrN) 及氮化鋁鈦(TiAlN) 最為常見，氮化鈦相較於氮化鉻，具有較 高的硬度，故多用於改善切削刀具的切削性能及增加使用壽命；而氮化鉻 雖然硬度不及氮化鈦，但在附著力、摩擦係數及抗氧化能力皆優於氮化鈦 薄膜，薄膜多應用於金屬成形模具。氮化鉻鈦矽(CrTiSiN) 複合薄膜在溫間 具有低摩擦係數、高硬度及良好的耐磨耗特性，另外，鎂合金之高強度及 重量輕等優點，使得其用途越來越廣泛，由於鎂合金其溫間成形性較佳， 故為了提升模具在溫間的模具壽命，以及降低磨耗、摩擦係數為目的，探 討溫間模具與薄膜之機械性質為近年來學者與業界努力的方向。

本研究使用陰極電弧沉積技術製備 CrTiSiN 複合薄膜，以掃描式電子 顯微鏡探討薄膜附著性及薄膜結構，之後使用有限元素分析法結合溫間奈 米壓痕實驗，求得溫間 CrTiSiN 複合薄膜之彈性係數、硬度、溫間應力-應 變曲線。其次，經溫間摩擦試驗機獲得複合層模具與鎂合金板材於石墨潤 滑下之摩擦係數，觀察溫間 CrTiSiN 薄膜與鎂合金之粗糙比，並與 TiAlN 薄膜比較。最後，以溫間磨耗試驗機，判斷不同鍍層在溫間下之耐磨耗性 及求得磨耗量與磨耗深度，並與業界常用之氮化鋁鈦薄膜比較。經實驗結果得知 SKD61 模具鋼，經過陰極電弧沉積系統鍍製 CrTiSiN 複合薄膜，硬度、耐磨耗性、摩擦係數有明顯的改善，其中 CrTiSiN 薄膜 在 300℃硬度最高，其值為 32.6 GPa，耐磨耗方面，常溫、高溫磨耗試驗結 果 CrTiSiN 比 TiAlN 耐磨耗，摩擦試驗方面，CrTiSiN 模具與鎂合金做純粹 壓平與滑動接觸後其鎂合金粗糙度皆比 TiAlN 低 ，由以上結果可顯示鍍上 CrTiSiN 薄膜能有效的降低摩擦係數，並改善表面耐磨耗性。

已決行

檔　　號：1903
保存年限：10

簽 於 機械與電腦輔助工程系105年5月19日

聯 絡 人：廖妙齡 （機械與電腦輔助工程系）
連絡方式：05-6315306 #5306
附　　件：Invitation letter_ThinFilms 2016_rev1.pdf、Tentative Conference Program.pdf、楊東昇老師簽名.pdf

主旨：擬請准予職(楊東昇)以公差假方式前往新加坡參加國際學術研討會議，敬請 鑒核。

說明：

一、『The 8th International Conference on Technological Advances of Thin Films & Surface Coatings (Thin Films 2016)』國際學術研討會議，將於105年7月12日至105年7月15日於新加坡舉行。

二、職投稿Thin Films 2016研討會之論文已被接受，接受函如附件，且獲邀論文發表，擬藉由此次出席國際會議之機會與國際人士切磋、交流與互動。

三、參加Thin Films 2016研討會所需註冊費及旅費約需新台幣10萬元左右，該經費擬由職之國科會計畫(104B071)及歷年計畫結餘款和管理費(共可勻支額300,000)支應，且變更原先規畫之歐、美等地區研討會為此研討會。

四、因行程關係，擬准105年7月11日啟程至新加坡、7月12-15日參加Thin Films 2016研討會及7月16日返程共6日請公差假，奉核後即進行辦理後續相關行政事宜。

第1頁　共2頁

國立虎尾科技大學
1055100419

圖一　簽呈

圖二　會場上之大型海報


TFS
The 8th International Conference on
Technological Advances of Thin Films & Surface Coatings
THINFILMS2016
12-15 JULY 2016, SINGAPORE
Schedule of ThinFilms 2016
薄膜大会 2016 会议流程
Date: 12-15 July 2016
Venue: Singapore Holiday Inn Atrium Singapore
Time 时间
Function 形式
July 12
2 PM
Registration
July 13
AM
Opening & Keynote
PM
Breakout Session
July 14
AM
Poster Session
PM
Breakout Session
Evening
Banquet
July 15: AM & PM
Breakout Session

圖三　會場上之議程表

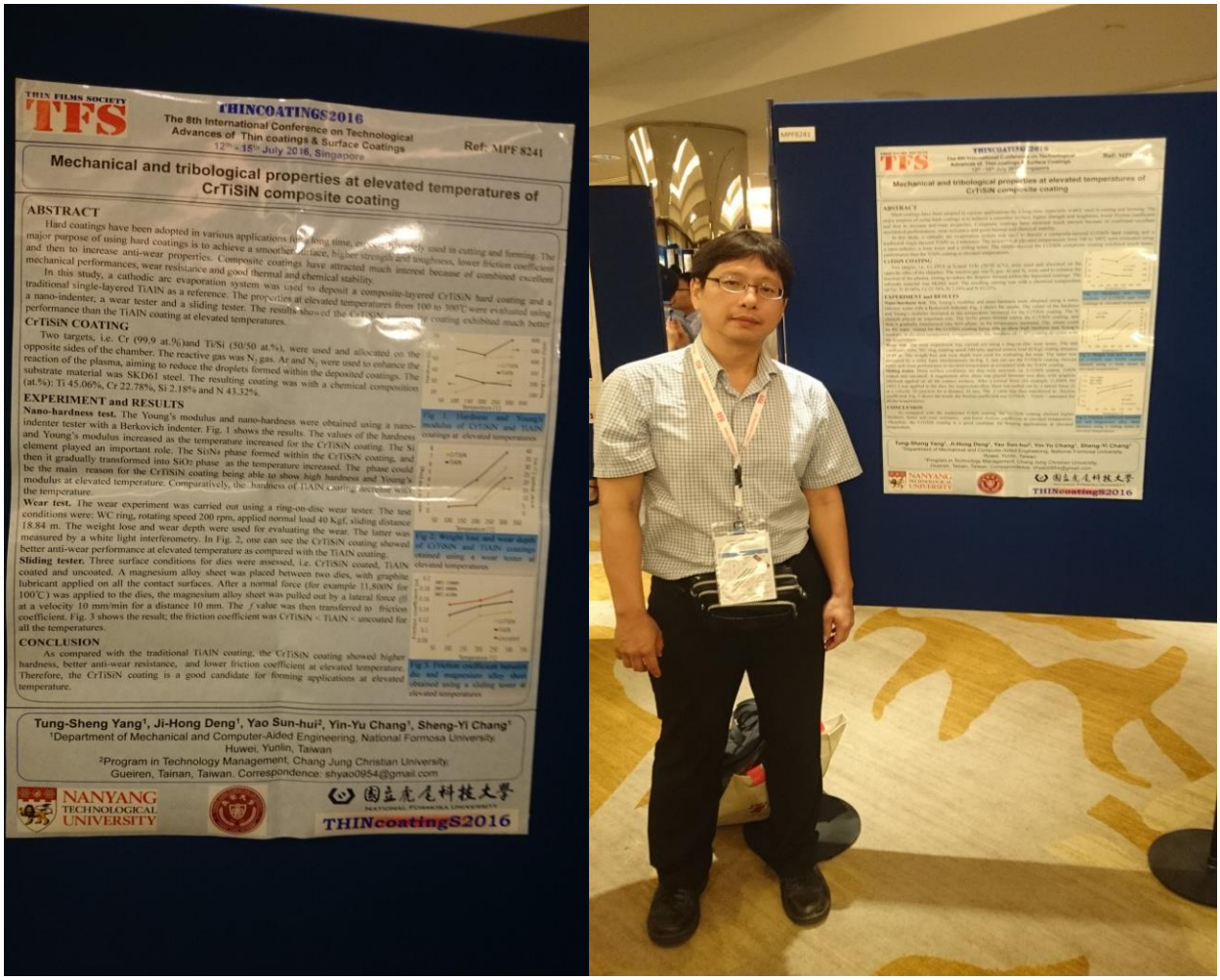

圖四 論文海報及本人參與研討會相片

microstructure of a-C:H films, and the microstructure is changed according to coating methods and parameters. In our previous study, Raman spectroscopy was used to clarify the microstructure of a-C:H films, and the microstructure of a-C:H films evaluated by Raman parameters (G-peak position and FWHM(G)) and the mechanical properties of the films were successfully correlated with Raman parameters. In this study, a-C:H films were prepared on Si wafer using plasma based ion implantation and deposition technique (PBII&D). Hardness of the films were measured with nanoindentor and surface roughness was measured using atomic force microscope. Ball-on-disc type tribotester was used to evaluate friction properties of the films in the air. It was found that the frictional properties of a-C:H films depend on their microstructure, i.e., polymer-like carbon (PLC), diamond-like carbon (DLC) and graphite-like carbon (GLC) structures, and PLC and GLC-structured a-C:H films show lower friction coefficients compared to that of DLC-structured carbon film, which are attributed to surface chemistry and low shear strength of the films, respectively. a-C:H films with DLC structure showed the highest friction coefficient and the friction coefficient increases in proportion to their hardness.

Presenter: Junho Choi (choi@mech.t.u-tokyo.ac.jp)
Corresponding author: Junho Choi (choi@mech.t.u-tokyo.ac.jp)

(MPF8241) Mechanical and tribological properties at elevated temperatures of CrTiSiN composite coating

Yang Tung-Sheng [1] , Deng Ji-Hong [2] , Yao shuen-huei [3] , Chang Yin-Yu [4] , Chang Sheng-Yi [5]
[1]Department of Mechanical and Computer-Aided Engineering, National Formosa University, Taiwan.
[2]Department of Mechanical and Computer-Aided Engineering, National Formosa University, Taiwan.
[3]Chang Jung Christian University, Program in Technology Management, Taiwan.
[4]Department of Mechanical and Computer-Aided Engineering, National Formosa University, Taiwan.
[5]Department of Mechanical and Computer-Aided Engineering, National Formosa University, Taiwan.

In this study, a composite-layered CrTiSiN hard coating was grown and evaluated for mechanical and tribological properties at elevated temperature. A traditional single-layered TiAlN was deposited and used for comparison. After the coatings were synthesized using a cathodic arc evaporation system, they were characterized. Then, the elastic-plastic stress-strain behavior, wear performance and friction behavior at elevated temperature from 100 to 300 ℃ were evaluated. The stress-strain behavior was derived from the comparison between load-displacement and pipe-up/sink-in behavior obtained by the finite element analysis and that by the nano-indentation test. The wear performance was assessed using a wear test. The friction behavior was investigated using a compressing and sliding test. The results showed that for the CrTiSiN coating, its hardness, Young's modulus and tangent modulus increased as the temperature increased. The CrTiSiN coating exhibited excellent anti-wear and low friction performance at elevated temperatures as compared to the TiAlN coating.

Presenter: Yao shuen-huei (shyao0954@gmail.com)
Corresponding author: Yao shuen-huei (shyao0954@gmail.com)

(MPF8263) Effects of SiC microparticles in electrolyte on structure and tribological property of micro-arc oxidation coatings of Ti6Al4V alloys

Fengbin Liu [1] , Dachao Sun [1] , Yan Cui [1]
[1]College of Mechanical and Materials Engineering, North China University of Technology, China.

Ti6Al4V alloy was widely used in the fields of aerospace and biological engineering for many excellent properties. However, the poor tribological behavior evidently hinders its further application. As an effective method, micro-arc oxidation technique was extensively carried out to improve the tribological properties of various nonferrous alloys because of its prominent advantages. Though wonderful effects were achieved by using micro-arc oxidation method, the typical porous morphology of micro-arc oxidation coating is still a disadvantage in improving the tribological behaviors.

圖五 研討會論文集之摘要部分

Mechanical and tribological properties at elevated temperatures of CrTiSiN composite coatings synthesized by a cathodic arc deposition process

Yang Tung-Sheng[1], Deng Ji-Hong[2] , Yao shuen-huei[3], Chang Yin-Yu[4] , Chang Sheng-Yi[5]

[1, 2, 4, 5]Department of Mechanical and Computer-Aided Engineering, National Formosa University, Taiwan.

[3]Chang Jung Christian University, Program in Technology Management, Taiwan.

Abstract

In this study, a cathodic arc evaporation process is used to deposit the traditional single-layered TiAlN and composite-layered CrTiSiN hard coatings. Field emission SEM is used to characterize the microstructure states of the synthesized films. Adhesion of the TiAlN and composite CrTiSiN films were evaluated using a standard Rockwell indentation tester. The hardness and Young's modulus were obtained by nanoindentation test. The stress-strain behavior such as yielding stress and tangent modulus of these deposited thin films were directly extracted by the comparison of load-displacement and pipe-up/sink-in behavior between the finite element analysis and the nanoindentation test at elevated temperatures. The results show the values of the hardness, Young's modulus, and tangent modulus increase as the temperature increases for CrTiSiN film. A wear test was used to determine the antiwear properties for different temperatures of these two deposited coatings. Pin-on-disk wear tests were conducted on the two deposited coated SKD61 steel disks using WC balls as sliding counter parts for different temperatures. The behavior of wear loses and the wear depths of these coatings were studied. The friction tests such as compressing and sliding test are carried out to investigate the variation of surface roughness and friction coefficient of magnesium alloy sheet for different temperatures. By comparison with the TiAlN film, the CrTiSiN composite thin films shows lower wear depth, surface roughness, and contact friction. Therefore, the CrTiSiN composite films exhibited excellent hardness, mechanical properties, surface quality, antiwear and low friction performance at elevated temperatures.

Keywords:hard coating, cathodic arc evaporation process, nanoindentation, mechanical properties, wear, friction, surface roughness, finite element analysis

1. Introduction

Hard coatings are adopted in cutting and forming application for a long time. The major purpose of hard coating is causing the smooth surface, increasing the strength and toughness, reducing the friction coefficient and increasing the antiwear properties. Industrial applications of these coatings in a form of single layer and multilayer synthesized by physical vapor deposition (PVD) are increasing rapidly due to their advanced tribological, corrosion properties, and high temperature oxidation resistance [1]. Such coatings can be produced by different PVD techniques, such as magnetron sputtering and cathodic-arc evaporation (CAE). The cathodic arc deposition technique possesses good adhesion and high deposition rate due to its high ionization and high current density as compared with other deposition processes [2]. TiN was widely used in the tool industry for protective coatings that provide increased wear resistance and cutting accuracy [3,4]. The demand of TiAlN film is expanding, because TiAlN film has a high oxidation resistance at elevated temperatures as well as good wear resistance [5]. The characteristic features of TiAlN coatings could be controlled by their chemical composition and microstructure, which significantly influence the mechanical properties of the deposited films [6]. Mo et al. [7] studied the tribological behaviors of the two commercially available high aluminum content TiAlN and AlCrN monolayer coatings, and they were investigated with focus on friction behaviors and wear mechanisms. Recently, composite coatings have attracted much interest because of their excellent mechanical performances, wear resistance, good thermal and chemical stability. Chang et al. [8, 9, 10] studied composite coatings synthesized by cathodic-arc evaporation equipment. The structure, mechanical and tribological property were investigated of these studies.

The well-known Rockwell C indentation test is prescribed by the VDI 3198 norm (Fig. 1), as a destructive quality test for coated compounds [11]. The results exhibited good, acceptable, and poor film adhesion for HF1～HF2, HF3～HF4, and HF5～HF6, respectively. The nanoindentation tests have been used to study the mechanical properties, such as elasticity, and hardness, of thin films with different film thicknesses and materials. Chang and Chang [12] used XPMTS nanoindentation with a Berkovich indenter, under load-unloading condition, and measured as a function of indenter displacement using continuous stiffness measurement method, to obtain the hardness and Young's modulus of the films. Recently, finite element method (FEM) has been widely used for numerical simulation of indentation tests on bulk and film material in order to analyze its deformation response and investigate the influence of indenter geometry, friction and material elastic and plastic properties. Pelletier et al. [13] have investigated the influence of material bilinear elastic-plastic behavior model for numerical simulation of nanoindentation testing of various bulk

metals. Pelletier [14] used a comprehensive parametric study of 48 cases was conducted. They defined two dimensionless equations which link the parameters extracted from the experimental load–displacement curve with material parameters, such as Young's modulus, yield stress and tangent modulus. Bhattacharya et al. [15] used the finite element method to simulate and solve for an indentation problem with an axisymmetric cone. They presented an elasto-plastic analysis of axisymmetric conical indentation, and showed that the shape of the plastic zone strongly depends on the indenter angle, Young's modulus of the material, and yield stress. Khan et al. [16] used nanoindentation test and finite element analysis to extract yield stress and strain hardening exponent for an Al-clad system. Yang et al. [17] used the finite element method in conjunction with an nanoindentation test to predict the loading curve and stress distribution of thin hard coatings. The effects of material properties of thin film on the stress distribution for loading and unloading in the nanoindentation are also investigated.

In this study, a cathodic arc evaporation process is used to deposit the traditional single-layered TiAlN and composite-layered CrTiSiN hard coatings. Field emission SEM is used to characterize the microstructure states of the synthesized films. Adhesion of the TiAlN and composite CrTiSiN films were evaluated using a standard Rockwell indentation tester. The stress-strain behavior such as Young's modulus, yielding stress, and tangent modulus of these deposited thin films were directly extracted by the comparison of load-displacement and pipe-up/sink-in behavior between the finite element analysis and the nanoindentation test at elevated temperatures. A wear test was used to determine the antiwear properties for different temperatures of these two deposited coatings. Pin-on-disk wear tests were conducted on the two deposited coated SKD61 steel disks using WC balls as sliding counter parts for different temperatures. The behavior of wear loses and the wear depths of these coatings were studied. The friction tests such as compressing and sliding test are also carried out to investigate the variation of surface roughness and friction coefficient of magnesium alloy sheet for different temperatures.

2. Microstructure and film adhesion analysis

The composite-layered CrTiSiN and single-layered TiAlN hard coatings were deposited on SKD61 tool steels by using a cathodic arc evaporation system. Ar and reactive gas (N2) were introduced through a conducting duct around the target to enhance the reaction of the plasma and reduce the droplet on the deposited coatings. Cr(99.9at%) for CrN and Ti/ Si+CrN (50/50 at.%) cathodes were arranged on opposite sides of the chamber to deposit the composite-layered CrTiSiN coatings. Ar and reactive gas (N2) were then introduced through a conducting duct around the

target to enhance the reaction of the plasma and reduce the droplet on the deposited coatings. The distance from cathode to substrate was 180 mm. The temperature of the sample during the deposition was controlled at about 200 °C, which was measured by a thermocouple located near the sample. Base pressure prior to deposition was lower than 1×10−3 Pa and substrate bias voltage of −120 V and N2 pressure of 2.7 Pa were used. Next, the samples were mounted on the rotational substrate holder for the deposition of the composite-layered CrTiSiN coatings. The rotational speed of the substrate holder was controlled at 4 rpm. Table 1 presents the deposition parameters of the composite-layered CrTiSiN coatings. In addition, the traditional single-layered TiAlN hard coatings also deposited using a cathodic arc evaporation system.

Cross-sectional structures of the deposited composite-layered CrTiSiN and TiAlN coatings were examined in a Joel JSM-7000F high resolution field emission scanning electron microscope (FESEM) equipped with secondary electron imaging (SEI) and backscattered electron imaging (BEI) detectors. The SEM micrograph obtained with backscattered electron detector emphasized the dissimilarity between CrTiSiN and TiAlN films. Figure 2 shows the Cross-sectional diagrams for composite-layered CrTiSiN and single-layered TiAlN coating, respectively. Total thickness of composite-layered CrTiSiN and single-layered TiAlN coatings was about 1.5μm (including 0.025μm Cr and 0.309μm CrN intermediate layers) and 1.519μm, respectively. Adhesion of the deposited coatings was assessed using a Rockwell-C indention hardness tester. It uses a standard Rockwell-C ball indenter, causing layered damage adjacent to the indentation boundary. After indentation, a secondary and backscattered SEM was used to evaluate the test. The indentation force (1471 N) is applied to the deposited coatings. Figure 3 shows the typical damage conditions of the deposited composite-layered CrTiSiN and TiAlN coatings. The failure mode and adhesion strength of the deposited coatings were evaluated using the damaged condition around the indentation crater. By comparison with the VDI 3198 norm, the deposited TiAlN and CrTiSiN coatings possessed HF2 and HF3 fracture mode, respectively. The TiAlN coating and CrTiSiN coating exhibited good film adhesion and acceptable film adhesion, respectively.

3. Mechanical properties

3.1 Young's modulus and hardness of film at elevated temperatures

Young's modulus and hardness of the thin film were obtained using Nano-indenter test (TI 950 TriboIndenter) with a Berkovich indenter for different high temperature. The maximum penetration depth was controlled at approximately 10%, therefore, the influence of substrate is negligible. The hardness of CrTiSiN film is 20.419 GPa, 29.1433 GPa, and 32.602 GPa at different elevated temperatures,

respectively. While the hardness of TiAlN film is 35.35 GPa, 29.94 GPa, and 28.64 GPa at different elevated temperatures, respectively. The Young's modulus of CrTiSiN film is 356.71 GPa, 424.51 GPa, and 439.94 GPa at different elevated temperatures, respectively. While the hardness of TiAlN film is 494.16 GPa, 449.21 GPa, and 594.58 GPa at different elevated temperatures, respectively. The values of the hardness and Young's modulus increase as the temperature increases for CrTiSiN film. In general, hardening of CrTiSiN film can be contributed to the introduction of silicon for high temperature, and decrease of grain sizes. The values of the hardness decrease as the temperature increases for TiAlN film. In addition, the hardness of CrTiSiN film is smaller than TiAlN film at 100℃, while the hardness of CrTiSiN film is greater than TiAlN film at 300℃. Table 2 lists the measured Young's modulus and hardness of CrTiSiN and TiAlN thin film for different high temperature.

3.2 elastic-plastic stress-strain behavior of film at elevated temperatures

Figure 4 shows the FE-model of the film-substrate system on the nanoindentation process simulated in DEFORM-2D. An axisymmetric cone with half-included angle of 70.3° in which the conical indenter has the same area function as a Berkovich tip was used. The movement of the indenter is constrained to within the thickness-direction of the film metal. Nanoindentation is performed under precise and continuous load and depth measurement during the loading and unloading process (Fig. 5 (a)). Figure 5(b) presents the stress-strain curve with bilinear constitutive law of a film material where **E** is the elastic modulus, $\mathbf{Y_0}$ is the yield stress, and **ET** is the tangent modulus. The analyses assume that the substrate and indenter are elastic-plastic and rigid. Only half of the indenter and bulk material was simulated since both the indenter and material were symmetrical. The nodes along the axis of rotation can move only along the *y*-axis and all nodes on the bottom of the mesh are fixed. Figure 6 shows the simulation of loading and unloading process for different bilinear stress-strain behavior can obtain the approximate loading-displacement curve. Hence the solution of stress-strain curve to obtain the loading-displacement curve is not unique. Finally, the stress-strain behavior such as Young's modulus, yielding stress, and tangent modulus of these deposited thin films was directly extracted by the comparison of load-displacement and pipe-up/sink-in behavior between the finite element analysis and the nanoindentation test for different high temperature. Figure 7 shows the experimental and simulated load-displacement curve and sink-in/pipe-up curve for the CrTiSiN film of 100℃ temperature. Fig. 7(a) shows different bilinear stress-strain behavior can obtain the approximate loading-displacement curve. Fig. 7(b) and (c) shows the solution of bilinear stress-strain curve can be directly extracted by the comparison of pipe-up/sink-in curves between the finite element analysis and

the nanoindentation test. The obtained result of bilinear stress-strain curve is about E=356.71GPa, Y0=29.4 GPa, ET=100GPa. Figure 8 shows the experimental and simulated load-displacement curve and sink-in/pipe-up curve for the CrTiSiN film of 200℃ temperature. Fig. 8(a) shows different bilinear stress-strain behavior can obtain the approximate loading-displacement curve of 200℃ temperature. Fig. 8(b) and (c) shows the experimental and simulated sink-in/pipe-up curve. By the comparisons of these curves, the solution of bilinear stress-strain curve can be directly extracted between the finite element analysis and the nanoindentation test. The obtained result of bilinear stress-strain curve is about E=356.71GPa, Y0=29.4 GPa, ET=100GPa for the CrTiSiN film of 200℃ temperature. Figure 9 shows the experimental and simulated load-displacement curve and sink-in/pipe-up curve for the CrTiSiN film of 300℃ temperature. Fig. 9(a) shows different bilinear stress-strain behavior can obtain the approximate loading-displacement curve of 300 ℃ temperature. Fig. 9(b) and (c) shows the experimental and simulated sink-in/pipe-up curve. By the comparisons of these curves, the solution of bilinear stress-strain curve can be directly extracted between the finite element analysis and the nanoindentation test. The obtained result of bilinear stress-strain curve is about E=439.94GPa, Y0=30.75 GPa, ET=430GPa for the CrTiSiN film of 300℃ temperature. Figure 10 shows the extracted bilinear stress-strain curve of CrTiSiN film for 100℃, 200℃ and 300℃. The effective stress increases as the temperature increases for the same effective strain. The results also exhibited the explanations for the hardness increases as the temperature increases (Table 2).

Figure 11 shows the experimental and simulated load-displacement curve and sink-in/pipe-up curve for the TiAlN film of 100℃ temperature. Fig. 11(a) shows different bilinear stress-strain behavior can obtain the approximate loading-displacement curve. Fig. 11(b) and (c) shows the solution of bilinear stress-strain curve can be directly extracted by the comparison of pipe-up/sink-in curves between the finite element analysis and the nanoindentation test. The obtained result of bilinear stress-strain curve is about E=494.16GPa, Y0=27.6GPa, and ET=300GPa. Figure 12 shows the experimental and simulated load-displacement curve and sink-in/pipe-up curve for the TiAlN film of 200℃ temperature. Fig. 12(a) shows different bilinear stress-strain behavior can obtain the approximate loading-displacement curve of 200℃ temperature. Fig. 12(b) and (c) shows the experimental and simulated sink-in/pipe-up curve. By the comparisons of these curves, the solution of bilinear stress-strain curve can be directly extracted between the finite element analysis and the nanoindentation test. The obtained result of bilinear stress-strain curve is about E=449.2GPa, Y0=17.25 GPa, and ET=275GPa for the TiAlN film of 200℃ temperature. Figure 13 shows the experimental and simulated

load-displacement curve and sink-in/pipe-up curve for the TiAlN film of 300℃ temperature. Fig. 13(a) shows different bilinear stress-strain behavior can obtain the approximate loading-displacement curve of 300℃ temperature. Fig. 13(b) and (c) shows the experimental and simulated sink-in/pipe-up curve. By the comparisons of these curves, the solution of bilinear stress-strain curve can be directly extracted between the finite element analysis and the nanoindentation test. The obtained result of bilinear stress-strain curve is about E=594.58GPa, Y0=18.0 GPa, and ET=260GPa for the TiAlN film of 300℃ temperature. Figure 14 shows the extracted bilinear stress-strain curve of TiAlN film for 100℃, 200℃ and 300℃. The tangent modulus decreases as the temperature increases for the same effective strain.

4. Tribological properties at elevated temperatures

4.1 wear of the CrTiSiN and TiAlN coatings

The wear experiment was carried out using a ball-on-disc wear tester. The rotating speed was 200 rpm, and the applied normal load was 40 Kg. The sliding distance was about 18.84 m. A WC ball was employed as the pin counterpart. A wear tester was employed to evaluate the level of cumulative wear on the CrTiSiN, and TiAlN coated test pieces (the substrate is SKD61) caused by abrasion for different high temperature. The weight loses and wear depth calculating by white light interferometry was used for evaluating the wear between the WC ball and the film deposited on SKD61 material. Table 3 presents parameters of wear test at elevated temperatures.

Figure 15 shows the weight lose and wear depth of CrTiSiN film and TiAlN film at different elevated temperatures. The weight lose was about 1.2mg and 1.6mg for CrTiSiN film and TiAlN film under 100℃, respectively. The wear depth was about 2.78 *um* and 2.96 *um* for CrTiSiN film and TiAlN film under 100℃, respectively. The weight lose was about 1.8mg and 4.2mg for CrTiSiN film and TiAlN film under 200℃, respectively. The wear depth was about 3.39 *um* and 4.59 *um* for CrTiSiN film and TiAlN film under 200℃, respectively. The weight lose was about 5.8mg and 7.8mg for CrTiSiN film and TiAlN film under 300℃, respectively. The wear depth was 15.7 *um* and 22.61 *um* for CrTiSiN film and TiAlN film under 300℃, respectively. The weight loses and wear depths of the CrTiSiN film were less than that of the TiAlN at elevated temperatures. The results indicated that the CrTiSiN coating possessed antiwear properties at high temperature by comparing with the TiAlN coating.

4.2 Friction test at elevated temperature

The friction tests including compressing and sliding conditions are carried out to

investigate the variation of coefficient of friction and surface roughness of magnesium alloy sheet at elevated temperatures. The CrTiSiN coating, TiAlN coating and absent coating are used in the friction test. The schematic diagram of compressing test was shown in Figure 16. The normal force is applied to the die and the magnesium alloy sheet is stationary. The normal force is 11800N, 8980N, and 6120N for 100℃, 200℃, and 300℃, respectively. The normal force is applied continuously for 1 minute. The three conditions of SKD61 die surface were CrTiSiN coating and TiAlN coating, and absent coating. The graphite lubricants applied to the contact surface between die and magnesium alloy sheet. Table 4 lists the parameters of the compressing test at the different elevated temperatures. Figure 17 shows the surface roughness ratio of magnesium alloy sheet under the compressing test at different elevated temperatures. The variation of surface roughness ratio (Ra'/Ra) of magnesium alloy sheet was investigated under the compressing test. The Ra is defined as the initial surface roughness, while the Ra' is defined as the surface roughness after compressing process. Fig. 17(a) shows the surface ratio of magnesium alloy sheet was 0.649, 0.693, and 0.909 for CrTiSiN film, TiAlN film and absent coating under the condition of 100°C temperature and 11800N normal force, respectively. Fig. 17(b) shows the surface ratio of magnesium alloy sheet was 0.663, 0.842, and 0.9503 for CrTiSiN film, TiAlN film and absent coating under the condition of 200°C temperature and 8980N normal force, respectively. Fig. 17(c) shows the surface roughness ratio of magnesium alloy sheet was 0.825, 0.913, and 1.006 for CrTiSiN film, TiAlN film and absent coating under the condition of 300°C temperature and 6120N normal force, respectively. The results shows the surface roughness ratio of magnesium alloy sheet was CrTiSiN < TiAlN < absent coating at the elevated temperatures. The CrTiSiN film shows the good surface quality of magnesium alloy sheet under compressing test.

The schematic diagram of sliding test was shown in Figure 18. The normal force is applied to the die and the magnesium alloy sheet moved with lateral velocity. The normal force is 11800N, 8980N, and 6120N for 100℃, 200℃, and 300℃ temperature, respectively. The lateral velocity is 10 mm/min and sliding distance is 10 mm. The three conditions of SKD61 die surface were CrTiSiN coating and TiAlN coating, and absent coating. The graphite lubricants applied to the contact surface between die and magnesium alloy sheet. Table 5 lists the parameters of the sliding test at the different elevated temperatures. The variation of surface roughness ratio (Ra'/Ra) of magnesium alloy sheet and the contact friction were investigated under the sliding test. Figure 19 shows the surface roughness ratio of magnesium alloy sheet under the sliding test at different elevated temperatures. Fig. 19 (a) shows the surface roughness ratio of magnesium alloy sheet was 0.672, 0.705, and 0.842 for CrTiSiN film, TiAlN film and absent coating under the condition of 100°C temperature and 11800N normal

force, respectively. Fig. 19 (b) shows the surface roughness ratio of magnesium alloy sheet was 0.691, 0.742, and 0.887 for CrTiSiN film, TiAlN film and absent coating under the condition of 200°C temperature and 8980N normal force, respectively. Fig. 19 (c) shows the surface roughness ratio of magnesium alloy sheet was 0.693, 0.835, and 0.877 for CrTiSiN film, TiAlN film and absent coating under the condition of 300°C temperature and 6120N normal force, respectively. The surface roughness ratio of magnesium alloy sheet was CrTiSiN < TiAlN < absent coating at different elevated temperatures. The CrTiSiN film shows the good surface quality of magnesium alloy sheet under sliding test.

Figure 20 shows the friction coefficient between die and magnesium alloy sheet under the sliding test at different elevated temperatures Fig. 20(a) shows the friction coefficient between of die and magnesium alloy sheet under the sliding test was 0.09, 0.13, and 0.15 for CrTiSiN film, TiAlN film and absent coating under the condition of 100°C temperature and 11800N normal force, respectively. Fig. 20(b) shows the friction coefficient between of die and magnesium alloy sheet under the sliding test was 0.13, 0.15, and 0.16 for CrTiSiN film, TiAlN film and absent coating under the condition of 200°C temperature and 8980N normal force, respectively. Fig. 20(c) shows the friction coefficient between of die and magnesium alloy sheet under the sliding test was 0.14, 0.16, and 0.18 for CrTiSiN film, TiAlN film and absent coating under the condition of 300°C temperature and 6120N normal force, respectively. The friction coefficient between the die and magnesium alloy sheet was CrTiSiN < TiAlN < absent coating at different elevated temperatures. Thus, the CrTiSiN film shows the small friction between die and magnesium alloy sheet under sliding test.

5. Conclusions

In this study, CrTiSiN and TiAlN coatings were synthesized by cathodic-arc evaporation. Rockwell-C adhesion test results indicated the criterion HF2–HF3 fracture mode of the deposited coatings, and exhibited sufficient film adhesion. Nanoindentation test results showed the hardness of CrTiSiN film was 20.419 GPa, 29.1433 GPa, and 32.602 GPa at different elevated temperatures, respectively. While the hardness of TiAlN film was 35.35 GPa, 29.94 GPa, and 28.64 GPa at different elevated temperatures, respectively. The values of the hardness increased as the temperature increased for CrTiSiN film. The values of the hardness decreased as the temperature increased for TiAlN film. In addition, the hardness of CrTiSiN film was smaller than TiAlN film at 100℃, while the hardness of CrTiSiN film was greater than TiAlN film at 300℃. The stress-strain behavior such as Young's modulus, yielding stress and tangent modulus of these deposited thin films were directly extracted by the comparison of load-displacement and pipe-up/sink-in behavior

between the finite element analysis and the nanoindentation test at elevated temperatures. The results show the values of the hardness, Young's modulus, and tangent modulus increase as the temperature increases for CrTiSiN film. The wear analyses of the CrTiSiN and TiAlN coatings deposited on SKD-61 tool steels was revealed by ball-on-disc wear tester with a WC ball as the pin counterpart. It showed the CrTiSiN coating possessed excellent antiwear properties as compared with the TiAlN coating at different elevated temperatures. The friction tests such as compressing and sliding test are carried out to investigate the variation of surface roughness and friction coefficient of magnesium alloy sheet. By comparison with TiAlN coatings, the CrTiSiN film shows the good surface quality and low friction coefficient at different elevated temperatures.

Acknowledgments:

The funding from the National Science Council of Taiwan under the contract NSC -102-2221-E-150 -011 is sincerely appreciated.

References:

[1] S. Paldey and S. C. Deevi, Single layer and multilayer wear resistant coatings of (Ti,Al)N: a review, Mater. Sci. Eng. A342 (2003) 58-79.

[2] A. Flink, T. Larsson, J. Sjolen, L. Karlsson, and L. Hultman, Influence of Si on the microstructure of arc evaporated (Ti,Si)N thin films; evidence for cubic solid solutions and their thermal stability, Surf. Coat. Technol. 200 (2005) 1535-1542.

[3] J. W. He, C. D. Bai, K. W. Xu, and N. S. Hu, Improving the anticorrosion and mechanical behaviour of PACVD TiN, Surf. Coat. Technol. 74-75 (1995) 387-393.

[4] A. G. Every, W. Pang, J. D. Comins, and P. R. Stoddart, Brillouin scattering study of guided modes in TIN films on high-speed steel, Ultrasonics 36 (1998) 223-227.

[5] C. W. Kim and K. H. Kim, Anti-oxidation properties of TiA1N film prepared by plasma-assisted chemical vapor deposition and roles of Al, Thin SoLid Fihns 307 (1997) 113-119.

[6] H. Ohnuma, N. Nihira, A. Mitsuo, K. Toyoda, K. Kubota, and T. Aizawa, Effect of aluminum concentration on friction and wear properties of titanium aluminum nitride films, Surf. Coat. Technol. 177 – 178 (2004) 623–626.

[7] J. L. Mo, M. H. Zhu, B. Lei, Y. X. Leng, and N. Huang, Comparison of tribological behaviours of AlCrN and TiAlN coatings—Deposited by physical vapor deposition, Wear 263 (2007) 1423–1429.

[8] Y. Y. Chang, S. J. Yang and D. Y. Wang, Structural and mechanical properties of

Cr–C–O thin films synthesized by a cathodic-arc deposition process, Surface & Coatings Technology 202 (2007) 941–945.

[9] Y. Y. Chang, S. J. Yang, and W. Wu, Plasma analyses and structural properties of Cr–N–C–O coatings synthesized by a cathodic arc evaporation process, Thin Solid Films 517 (2009) 4238–4241.

[10] S. M. Yang, Y. Y. Chang, D. Y. Lin, D. Y. Wang and W. Wu ,Mechanical and tribological properties of multilayered TiSiN/CrN coatings synthesized by a cathodic arc deposition process, Surface & Coatings Technology 202 (2008) 2176–2181.

[11] Verein Deutscher Ingenieure Normen, VDI 3198, VDI-Verlag, Dusseldorf, (1991).

[12] Y.Y. Chang, C. P. Chang, Microstructural and mechanical properties of graded and multilayered AlxTi1-xN/CrN coatings synthesized by a cathodic-arc deposition process, Surface & Coatings Technology 204 (2009) 1030–1034.

[13] H. Pelletier, J. Krier, A. Cornet, P. Mille, Limits of using bilinear stress]strain curve for finite element modeling of nanoindentation response on bulk materials, Thin Solid Films 379 (2000) 147-155.

[14] H. Pelletier, Predictive model to estimate the stress–strain curves of bulkmetals using nanoindentation, Tribology International 39 (2006) 593-606.

[15] A. K. Bhattacharya, W. D. Nix, Finite element analysis of cone indentation, Inte. J. of Solids and Structures 27(1991) 1047-1058.

[16] M.K. Khan, S.V. Hainsworth, M.E. Fitzpatrick, L. Edwards, A combined experimental and finite element approach for determining mechanical properties of aluminium alloys by nanoindentation, Computational Materials Science 49 (2010) 751-760.

[17] T. S. Yang, S. Y. Chang and J. H. Deng, Investigation of loading-unloading curve and stress distribution of thin hard coating by finite element analysis during nanoindentation process, Applied Mechanics and Materials, Vols. 465-466 (2014) pp 1365-1369,

Table 1 deposition parameters of the CrTiSiN coatings

Coating type	CrTiSiN
Target	Cr(99.9at%)for CrN, 50Ti-50Si+CrN
Reaction gas	N_2
Distance between cathode to substrate (mm)	180
Evaporate current (A)	60
Substrate bias (V)	-120
Substrate temperature (℃)	200
Deposition time (min)	40
Rotation (rpm)	4

Table 2 experimental results of hardness and Young's modulus (nanoindentation test)

Test pieces	Hardness(H)	Young's modulus (E)
100℃-CrTiSiN	20.419 GPa	356.71GPa
200℃-CrTiSiN	29.1433 GPa	424.51 GPa
300℃-CrTiSiN	32.602 GPa	439.94 GPa
100℃-TiAlN	35.35 GPa	494.16 GPa
200℃-TiAlN	29.94 GPa	449.21 GPa
300℃-TiAlN	28.64 GPa	594.58 GPa

Table 3 Parameters of wear test at elevated temperatures

	100℃	200℃	300℃
normal force	40Kg	40Kg	40Kg
rotation speed	200rpm	200rpm	200rpm
material of pin	WC	WC	WC
sliding distance	18.84 m	18.84 m	18.84 m

Table 4 Parameters of the compressing test (sheet is stationary)

	100℃	200℃	300℃
normal force	11800N	8980N	6120N
time of continuous force	1 min	1 min	1 min

Table 5 Parameters of the sliding test

	100℃	200℃	300℃
normal force	11800N	8980N	6120N
sliding distance	10mm	10mm	10mm
sliding velocity	10 mm/min	10 mm/min	10 mm/min

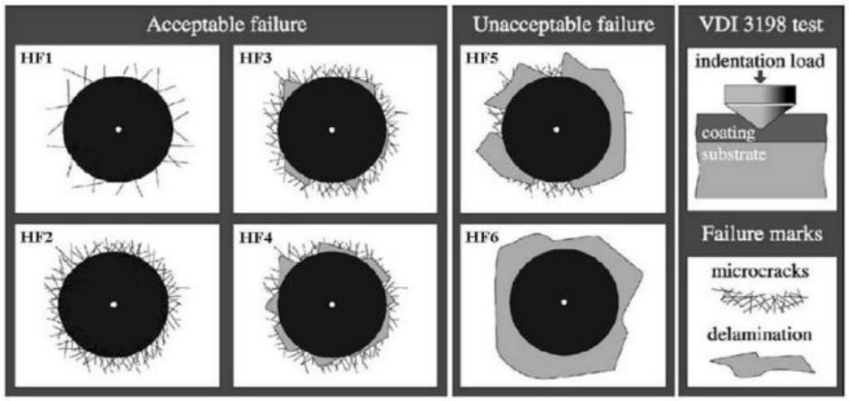

Fig.1 VDI 3198 norm

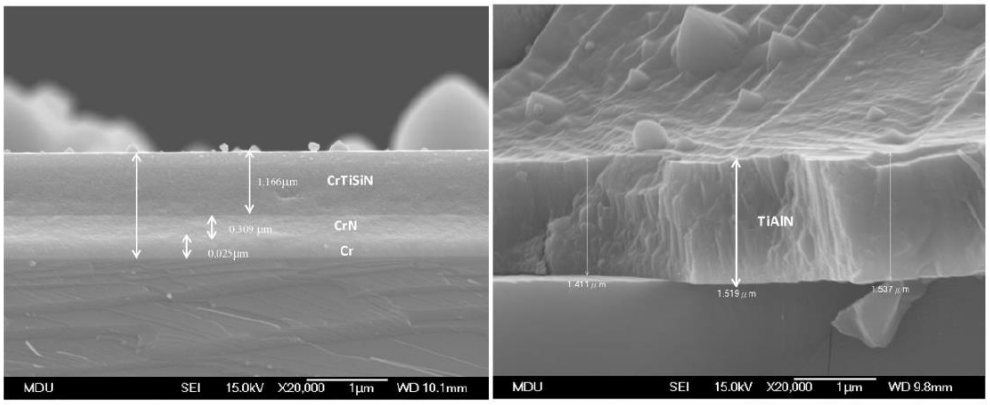

(a) CrTiSiN (b) TiAlN

Figure 2 CrTiSiN and TiAlN cross-sectional diagram by SEM

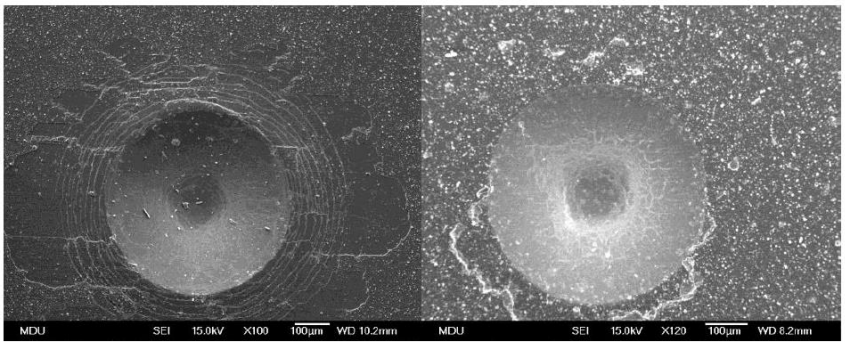

(a) CrTiSiN film (b) TiAlN film

Figure 3 CrTiSiN-SEM images and TiAlN-SEM images of Rockwell indentationof Rockwell indentation

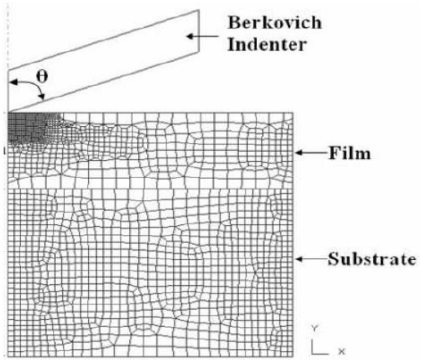

Figure 4 FE-model of the film-substrate system on the nanoindentation process

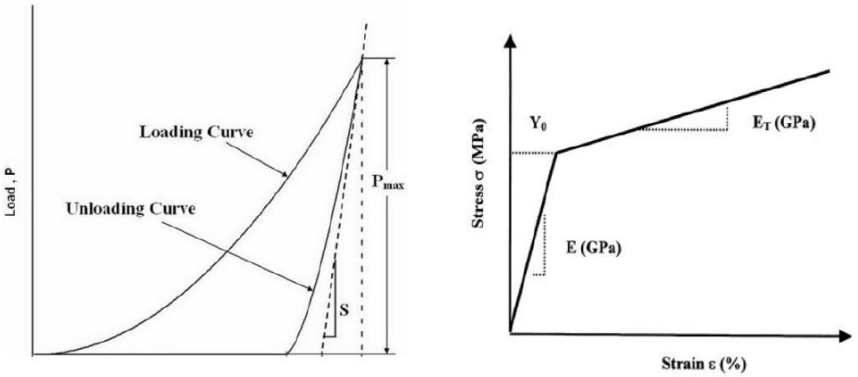

(a) load and unloading curve (b) bilinear stress-strain curve

Figure 5 loading-unloading curve and bilinear stress-strain curve

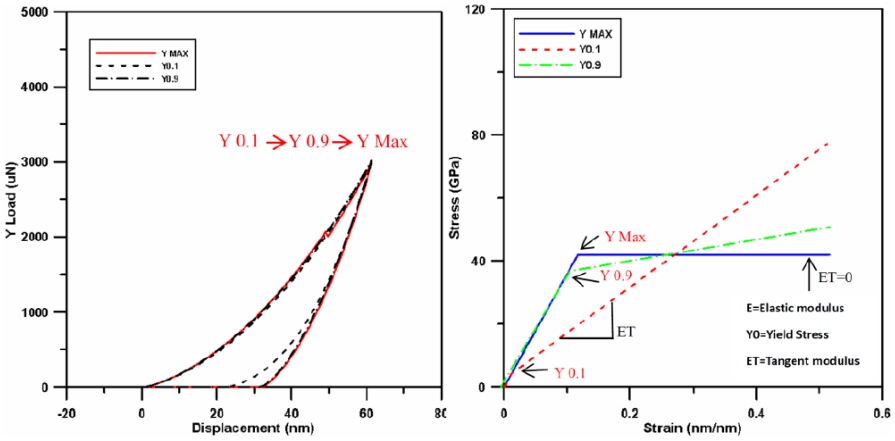

(a) simulated loading-displacement curve (b) different bilinear stress-strain curve

Fig. 6 simulation of loading and unloading process for different bilinear stress-strain behavior can obtain the approximate loading-displacement curve

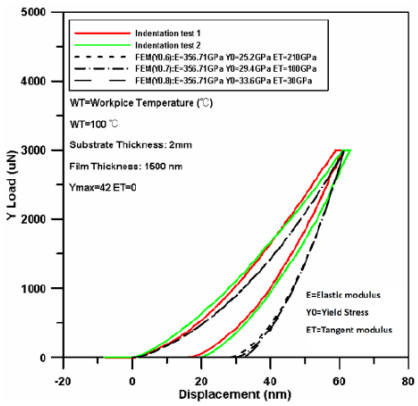

(a) experimental and simulated load-displacement curve

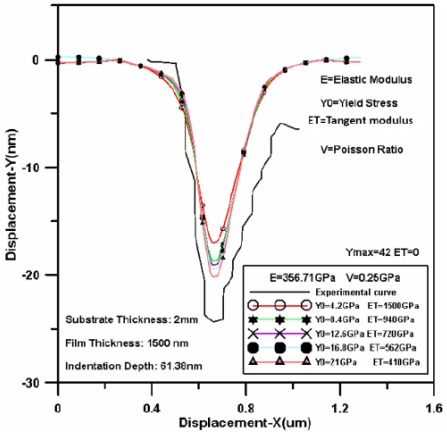

(b) experimental and simulated sink-in/pipe-up curve (Y_0=4.2GPa-21GPa)

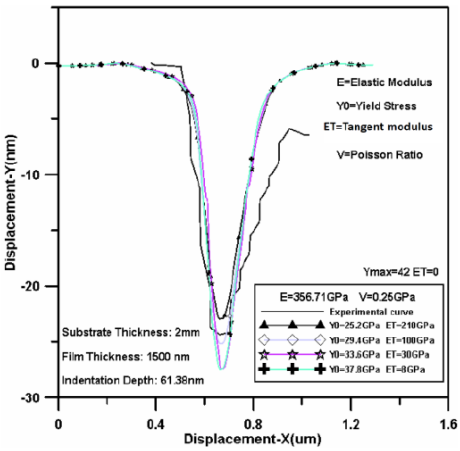

(c) experimental and simulated sink-in/pipe-up curve (Y_0=25.2GPa-37.8GPa)

Fig. 7 Comparison of experimental and simulated load-displacement curve and sink-in/pipe-up curve for the CrTiSiN film of 100℃ temperature (Result: E=356.71GPa, Y0=29.4 GPa, ET=100GPa)

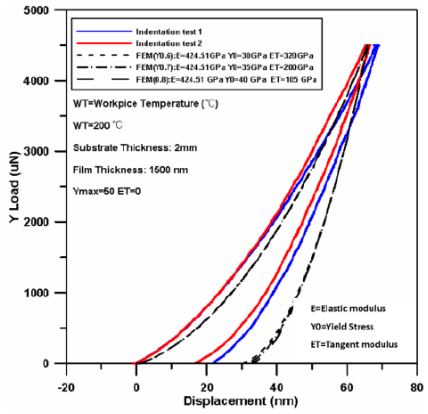

(a) experimental and simulated load-displacement curve

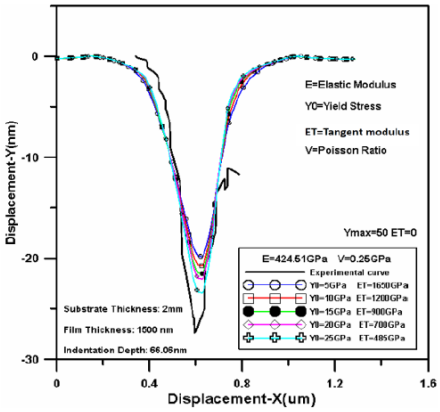

(b) experimental and simulated sink-in/pipe-up curve (Y_0=5.0GPa-25GPa)

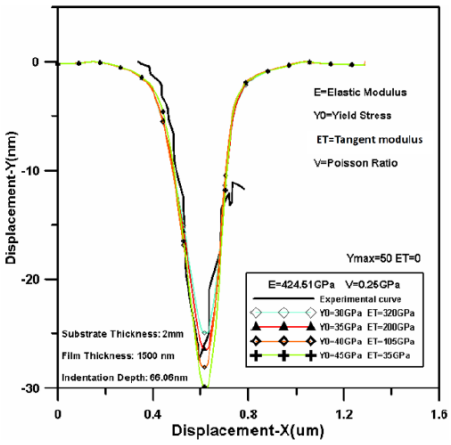

(c) experimental and simulated sink-in/pipe-up curve (Y_0=30.0GPa-45.0GPa)

Fig. 8 Comparison of experimental and simulated load-displacement curve and sink-in/pipe-up curve for the CrTiSiN film of 200℃ temperature (Result: E=424.51GPa, Y0=35 GPa, ET=200GPa)

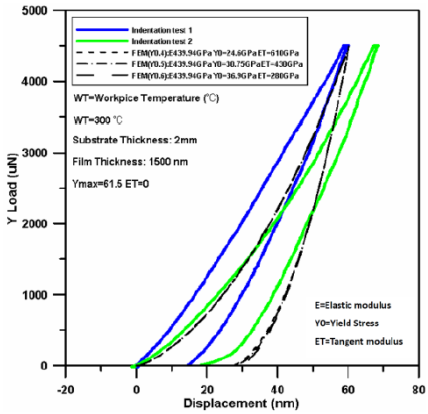

(a) experimental and simulated load-displacement curve

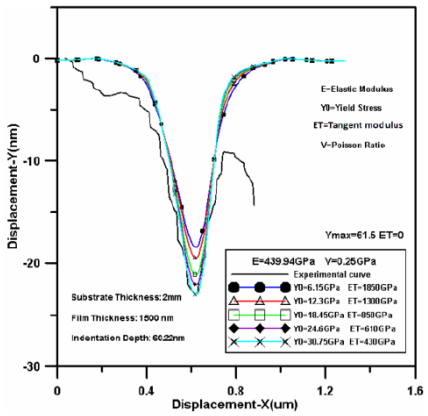

(b) experimental and simulated sink-in/pipe-up curve (Y_0=5.0GPa-25GPa)

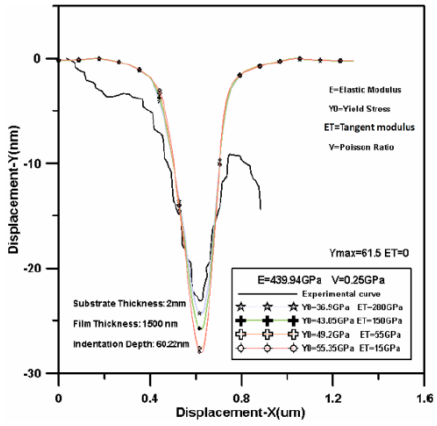

(c) experimental and simulated sink-in/pipe-up curve (Y_0=30.0GPa-45.0GPa)

Fig. 9 Comparison of experimental and simulated load-displacement curve and sink-in/pipe-up curve for the CrTiSiN film of 200℃ temperature (Result: E=439.94GPa, Y0=30.75 GPa, ET=430GPa)

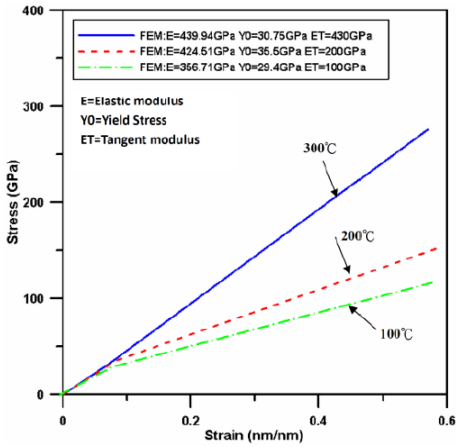

Fig. 10 extracted bilinear stress-strain curve of CrTiSiN film for 100℃-300℃

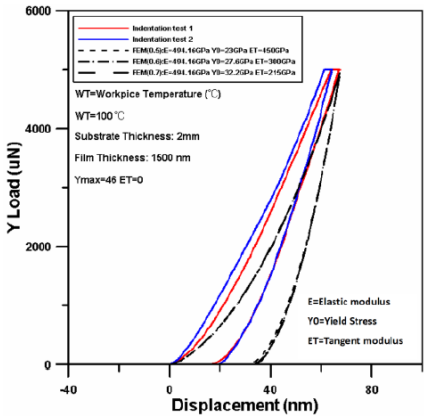

(a) experimental and simulated load-displacement curve

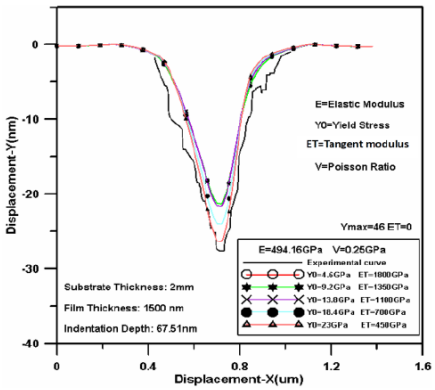

(b) experimental and simulated sink-in/pipe-up curve (Y_0=4.6GPa-23GPa)

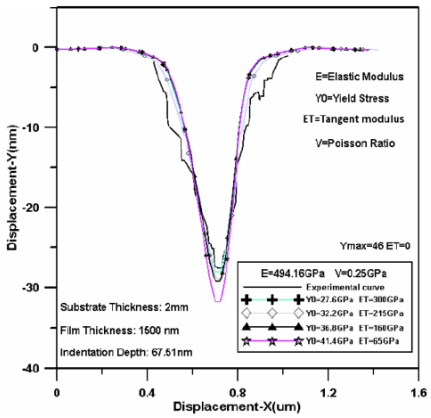

(c) experimental and simulated sink-in/pipe-up curve (Y_0=27.6GPa-41.4GPa)

Fig. 11 Comparison of experimental and simulated load-displacement curve and sink-in/pipe-up curve for the TiAlN film of 100℃ temperature (Result: E=494.16GPa, Y0=27.6 GPa, ET=300GPa)

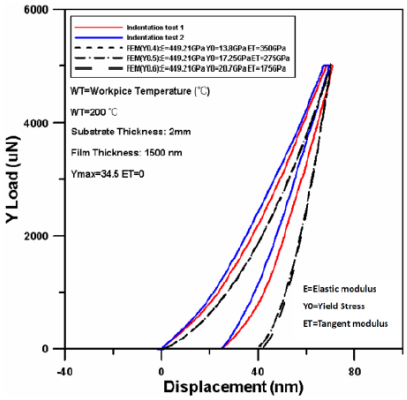

(a) experimental and simulated load-displacement curve

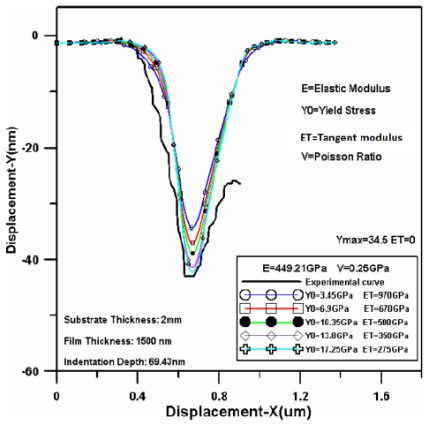

(b) experimental and simulated sink-in/pipe-up curve (Y_0=3.4GPa-17.25GPa)

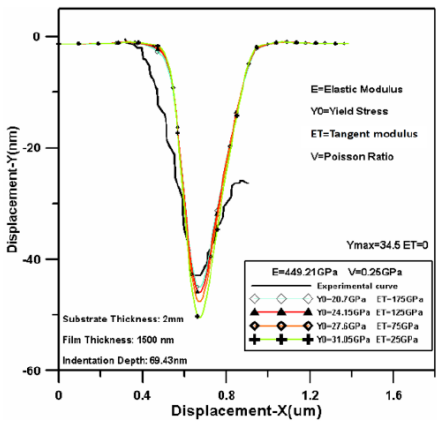

(c) experimental and simulated sink-in/pipe-up curve (Y_0=20.7GPa-31.05GPa)

Fig. 12 Comparison of experimental and simulated load-displacement curve and sink-in/pipe-up curve for the TiAlN film of 200℃ temperature (Result: E=449.2GPa, Y0=17.25 GPa, ET=275GPa)

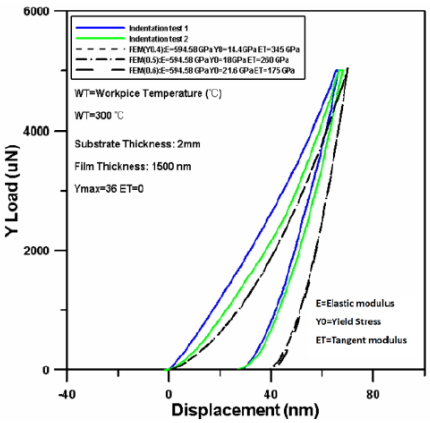

(a) experimental and simulated load-displacement curve

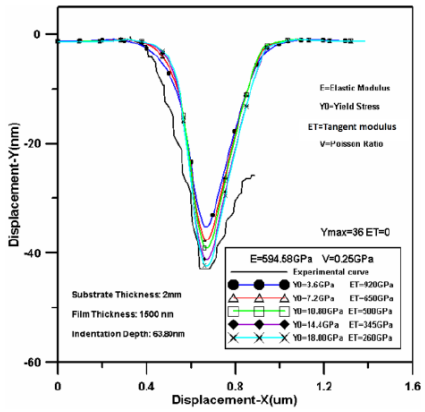

(b) experimental and simulated sink-in/pipe-up curve (Y_0=3.6GPa-18.0GPa)

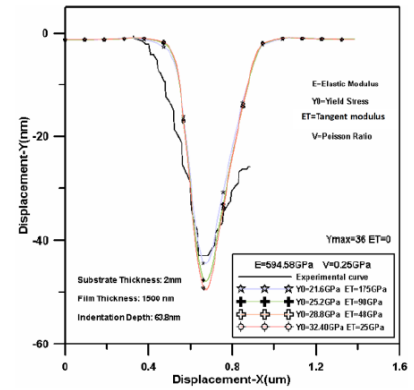

(c) experimental and simulated sink-in/pipe-up curve (Y_0=21.6GPa-32.40GPa)

Fig. 13 Comparison of experimental and simulated load-displacement curve and sink-in/pipe-up curve for the TiAlN film of temperature

(Result: E=594.58GPa, Y0=18.0 GPa, ET=260GPa)

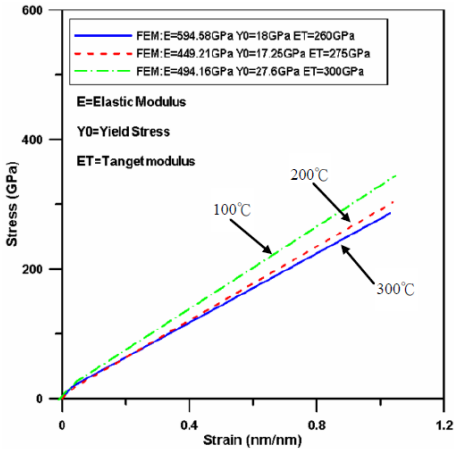

Fig. 14 extracted bilinear stress-strain curve of TiAlN film for 100℃-300℃

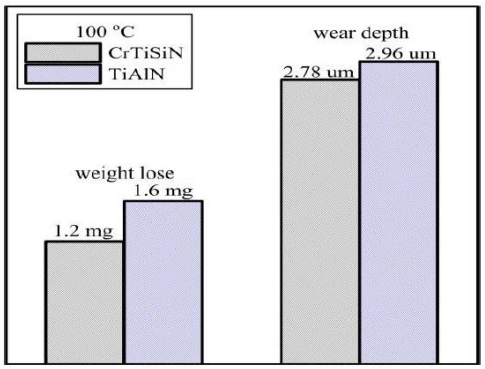

(a) 100℃

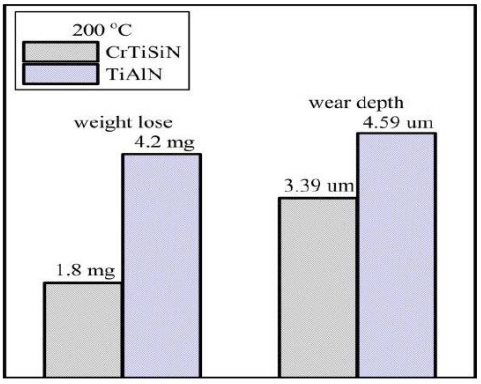

(b) 200℃

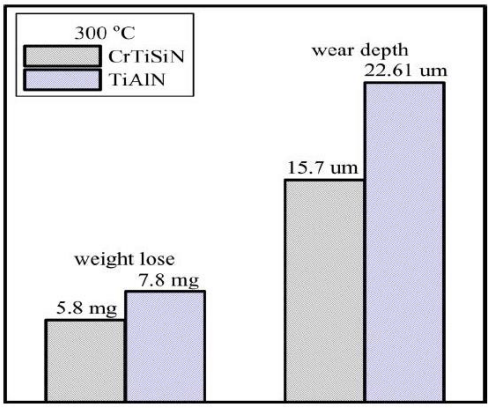

(c) 300℃

Fig. 15 Weight lose and wear depth of CrTiSiN film and TiAlN film at different elevated temperatures

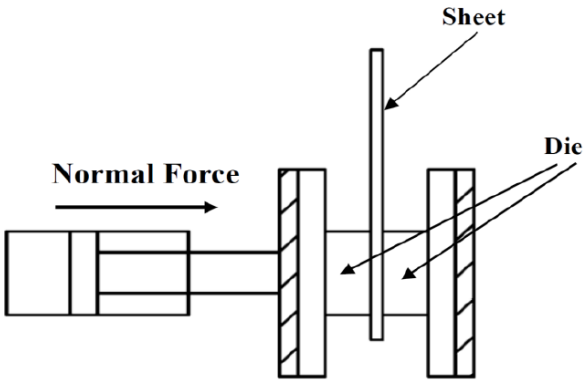

Fig. 16 Schematic diagram of compressing test

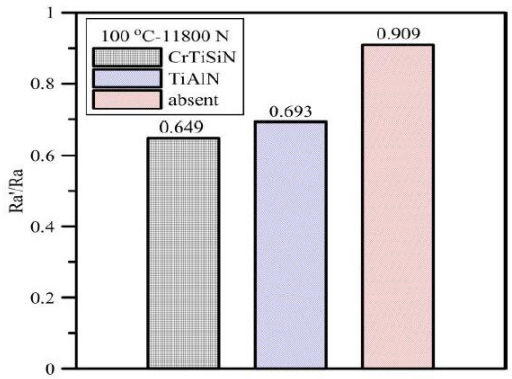

(a) 100°C temperature and 11800N normal force

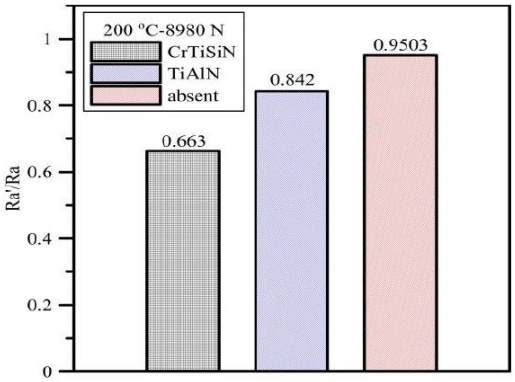

(b) 200°C temperature and 8980N normal force

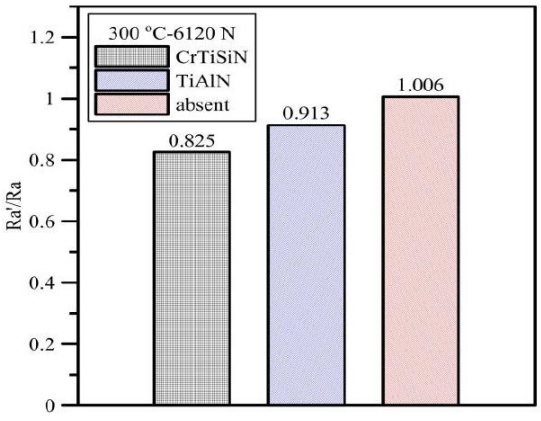

(c) 300°C temperature and 6120N normal force

Fig. 17 Surface roughness ratio of magnesium alloy sheet under the compressing test at different elevated temperatures

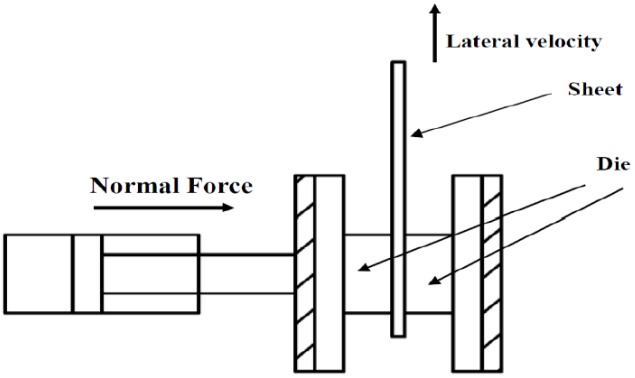

Fig. 18 Schematic diagram of sliding test

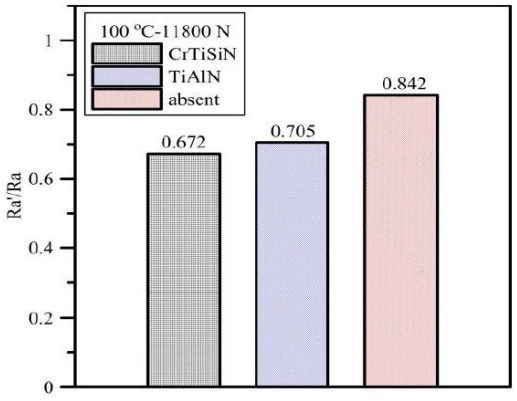

(a) 100°C temperature and 11800N normal force

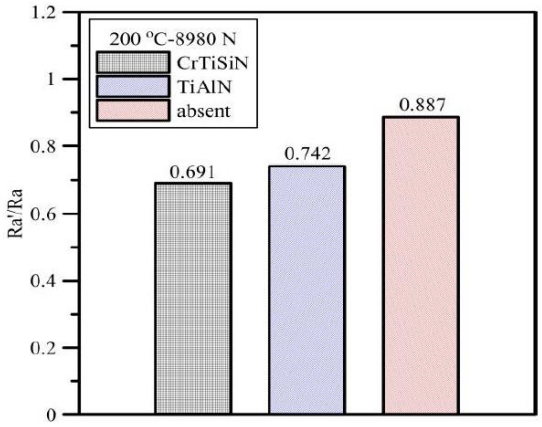

(b) 200°C temperature and 8980N normal force

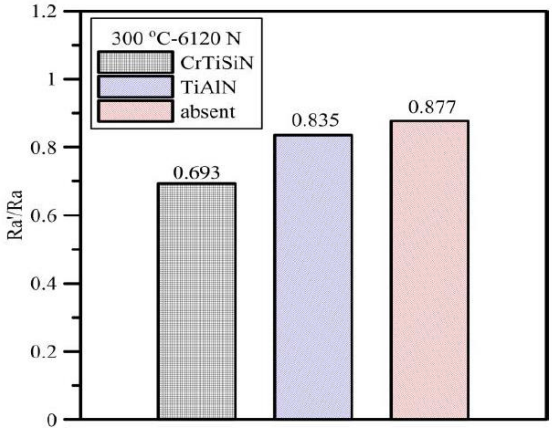

(c) 300°C temperature and 6120N normal force

Fig. 19 Surface roughness ratio of magnesium alloy sheet under the sliding test at different elevated temperatures

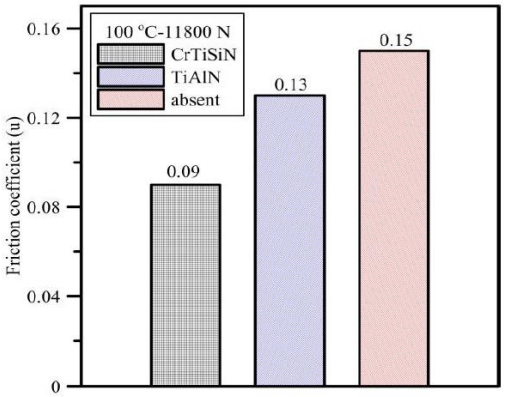

(a) 100°C temperature and 11800N normal force

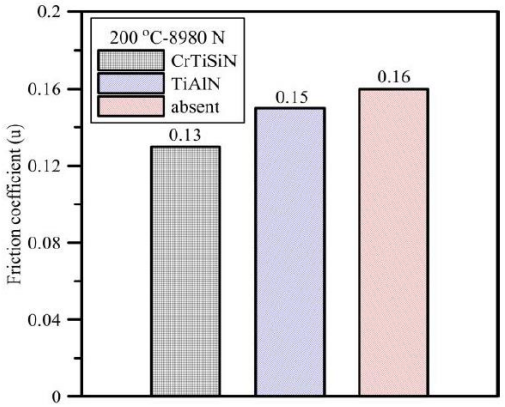

(b) 200°C temperature and 8980N normal force

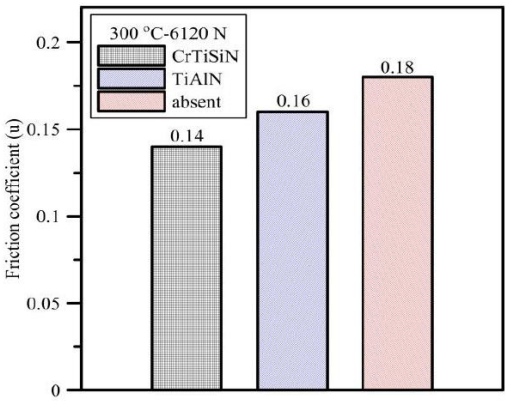

(c) 300°C temperature and 6120N normal force

Fig. 20 Friction coefficient between die and magnesium alloy sheet under the sliding test at different elevated temperatures

29

圖六 此次發表文章之內容

心得與建議

本次參與 Thin Films 2016 會議心得與建議如下：

1. 此會議中有多篇論文有開發新的薄膜，也應用於不同的產業，而本身之領域為應用於模具表面之硬質鍍層薄膜，希望能增加模具之壽命，也其一些先進薄膜更是能提高模具壽命，值得學習與研究，期能藉此提升自己之產學能量、精進研究方法。
2. 藉由此次參與會議了解薄膜之先進技術及應用於業界，因此可將薄膜應用於模具方面之新知帶給學生，促進教學成效。